Int. J. Multiphase Flow Vol. 15, No. 3, pp. 357–370, 1989
Printed in Great Britain.

0301-9322/89 $3.00 + 0.00

NUMERICAL INVESTIGATION OF LARGE WAVE INTERACTIONS ON FREE FALLING FILMS

F. K. WASDEN and A. E. DUKLER
Department of Chemical Engineering, University of Houston, Houston, TX 77204, U.S.A.

(*Received* 21 *October* 1988; *in revised form* 15 *November* 1988)

Abstract—From experimental measurements of a free falling liquid film at Re = 880, four representative large, evolving or interacting waves were selected for computational domains in which the Navier–Stokes equations were numerically solved. The algorithm computed velocity and pressure fields within each wave, as well as the shape necessary to match experimental wall shear stress data. Results show interaction effects significantly modify flow fields, compared to large solitary waves. Waves having two peaks had two closed recirculation regions, with a mixing layer separating them. The size of the recirculation regions was dependent on the extent of separation of the wave peaks. As with solitary waves, strong streamwise accelerations exist, with both location and magnitude varying with shape and evolutionary character of the wave. Heat and mass transfer rates must be enhanced by these flow properties, which are shown to have a complicated dependence on wave structure. Examination of the flow fields suggests parabolic streamwise velocity profiles are generally deficient, explaining shortcomings experienced by hydrodynamic models based on such simple velocity profiles.

Key Words: falling liquid films, numerical methods

INTRODUCTION

Investigations of hydrodynamic and transport properties of thin falling liquid films remain a fertile research area today. Thin liquid films are encountered in a wide variety of industrial process equipment, including wetted wall absorbers, falling film chemical reactors, condensers and vertical tube evaporators. At flowrates of industrial interest, falling films (even in the absence of gas flow) evolve to a highly irregular wavy interface which is generally considered quasi-stationary. Figure 1 displays a short time trace of such a falling film, 10,000 mean film thicknesses below the inlet. The film surface is covered by a complex array of large and small waves moving over a substrate which is less than the mean film thickness. The large waves, ranging in amplitude from 2 to 5 times the substrate thickness, carry a large fraction of the total mass flowing, and are speculated to control the rates of scalar transport (Dukler 1977). Before the heat or mass transfer rates to such films can be modeled it is necessary to understand the velocity distributions which exist within these waves, as well as the evolution of the interface. The present work focuses on these questions.

Previous modeling efforts generally were limited to either single, non-interacting (solitary) waves of various thicknesses, or the intersection of small waves. While large, solitary waves and small ripples on the substrate symbolize asymptotic behavior of the flow, examination of film thickness measurements, as in figure 1, shows these limiting cases are not representative of the flow. Numerical simulation of the isolated, large waves at the flow conditions of figure 1 (Wasden & Dukler 1989) suggests transport through the film is enhanced by the interaction of large wave peaks with the relatively slowly moving substrate. This same study determined that the seemingly slow evolution of these waves is responsible for significant deviations in the flow field from those determined for solitary waves. The more complicated case of rapidly evolving or interacting waves integrates large wave interactions with the surrounding substrate and the potentially more important effects of wave interactions.

Evolution of the large waves far from the inlet may be regarded as processes of coalescence or splitting, and result from some type of flow instability. Large waves do not grow without limit, but split into daughter waves when sufficiently perturbed. Many large waves overrun smaller, slower moving waves, sometimes incorporating the smaller wave, while often passing over them

without significant mass addition. The wide array of large wave behavior illustrates the need for local measurements to determine relative effects of wave evolution and large wave induced convection on transport enhancement.

Reliable experimental measurements of the velocity distribution in the films is exceedingly difficult due to the extremely small film thickness (≈ 1 mm), very short passage time of each wave (≈ 60 ms) and the random location of the interface, as shown in figure 1. Non-intrusive methods, such as LDA, do not provide sufficiently fine resolution to investigate velocity profiles. Thus, experimental measurements of hydrodynamic variables appear limited to the time variation of wall shear stress and film thickness. Correspondingly, analytical models have been developed in the absence of hard data on the true flow conditions which appear to exist in the waves.

Most analytical models of both single and interacting waves extend the concepts advanced by Kapitza (1964), based on the use of a parabolic velocity profile and assuming that the streamwise hydrodynamic variables scale with the wavelength. In 1972, in examining various models developed to that date, Dukler concluded that all failed to accurately represent any measured characteristics of the wave except at Reynolds numbers well below those of industrial interest.

Modeling the wavy film flow by a direct solution of the Navier–Stokes equations is hampered by numerical stiffness imposed by the stress-free interface; as a result, convergence is difficult except at the lowest flowrates. Previous numerical modeling has focused solely on non-interacting large waves. Bach & Villadsen (1984) explored the application of a finite element scheme to the unsteady problem of solitary waves developing from initial perturbations on the smooth film for Reynolds numbers up to 100. The film Reynolds number is defined as $\mathrm{Re} = 4\,Q/\nu$, where Q is the mass flowrate per unit perimeter and ν is the kinematic fluid viscosity. Their work predicted that the flow far from the inlet would consist of solitary waves having one general shape, a condition contrary to experimental fact even at film Reynolds numbers as low as 1. Kheshgi & Scriven (1987) applied a finite element technique to a problem with periodic boundary conditions in the flow direction, and verified the evolution of infinitesimal disturbances as predicted by Orr-Sommerfeld analyses. Their work was limited to low flowrates, and failed to generate waveforms comparable to those observed experimentally for fully-developed flow.

Recent simulations of solitary waves at a high Reynolds number (880) proceeded by solving the Navier–Stokes equations in a partially determined flow domain (Wasden & Dukler 1989). This work showed that isolated wave velocity is strongly dependent on wave shape, and provided evidence that numerous streamwise length scales existed in the flow. Further, it was determined that effects of wave evolution are important near the solid boundary, shifting the maximum wall shear stress in front of the film thickness peak. The use of a parabolic streamwise velocity profile to describe the flow in large waves was shown to be inappropriate over a large portion of these waves, suggesting analytical models based on such velocity profiles are fundamentally inadequate.

At present, no suitable models for evolving waves exist. In the absence of such models, and experimental methods for measuring velocity profiles in thin wavy films, a series of numerical experiments was performed. The experiments propose to illuminate the subject of transport

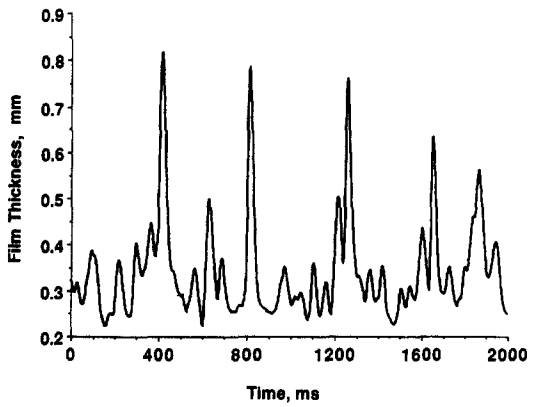

Figure 1. Film thickness time trace: Re = 880.

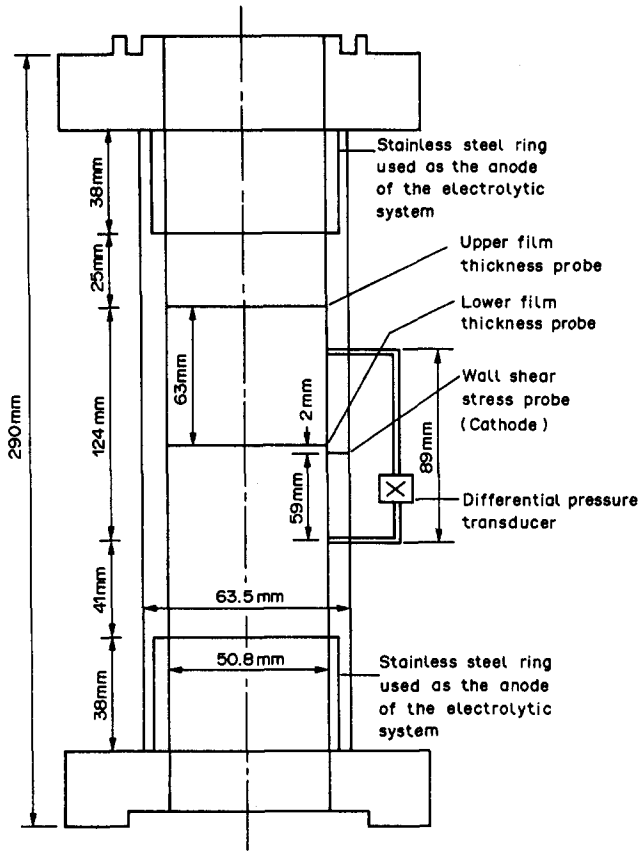

Figure 2. Measuring station.

enhancement due to waves by solving for the hydrodynamics within typical experimentally determined waveforms. For a film Reynolds number of 880, wave shapes and wall shear stress data were measured in our laboratory. Four representative large, interacting or evolving waveforms were converted for use as domains for a finite-difference code developed specifically for free surface problems. The use of experimentally measured waveforms is a novel concept, providing a somewhat simpler numerical task while insuring the results will not represent isolated or idealized cases of film flow. The results of these computations demonstrate the transport enhancement properties peculiar to evolving large waves, and present data useful for future model development.

EXPERIMENTAL PROCEDURE

Flow loop

For fully-developed wavy film flow, film thickness and wall shear stress data were collected in a 50.8 mm i.d. vertical test section in a flow loop described by Zabaras *et al.* (1986). After being pumped through a calibrated rotameter, the fluid entered the column through an annulus whose inner wall consists of a stainless steel porous sinter, having 100 μm pore size. Combined with careful leveling of the column prior to data collection, this entry section ensured minimal deviations from axisymmetric flow, and produced a smooth inlet flow. The measuring station was located 3.1 m (roughly 10,000 mean film thicknesses) below this entry section.

Measuring station and measurement techniques

The measuring station, shown in figure 2, is patterned after that described by Zabaras *et al.* (1986). The removable section allows simultaneous measurement of film thickness and wall shear stress at one location, as well as film thickness at another. The station was constructed of the same material as the flow loop, and was carefully machined to ensure a smooth transition to the station.

Film thickness probes consisted of twin parallel platinum–13% rhodium wires, 0.05 mm dia spaced 2.5 mm apart, which penetrated the flow. Described in detail by Brown *et al.* (1978), a linear relation exists between the resistance of the film between the wires and the film thickness. Calibration proceeded by setting the measuring station horizontal, blocking the ends and introducing different fluid levels, determined to within 10 μm using a cathetometer, followed by measurement of the resulting resistance. Downstream electronics for converting this resistance to a d.c. voltage signal are described elsewhere (Zabaras *et al.* 1986). Conductance of the fluid was monitored closely at all times during the calibration and data collection procedures to insure proper correction of any thermally induced conductance drift.

Wall shear stress measurements were based on the electrochemical mass transfer method described by Hanratty & Campbell (1983). For the present series of measurements, the iodine/tri-iodide system was chosen. The working solution contained 0.1 M KI and 0.004 M I_2(s) in demineralized water, and was replaced every 2 h to minimize errors due to iodine evaporation. A dry nitrogen atmosphere was used in the flow loop to minimize oxygen saturation of the solution. Fluid properties at 25 °C are: density, 1010 kg/m^3; absolute viscosity, 8.5×10^{-4} kg/m s; and surface tension, 7.12×10^{-2} N/m. The cathode for this system consists of a flush-mounted strip of platinum foil, 0.075 mm (in the flow direction) × 1 mm wide, embedded in Plexiglas to insure electrical isolation. By measuring the current produced by an electrochemical reaction at the surface of the cathode, the wall shear stress at that location is determined. For the redox reaction

$$I_3^- + 2e \rightarrow 3I^- \text{ (cathode)},$$

$$3I^- \rightarrow I_3^- + 2e \text{ (anode)},$$

a concentration boundary layer develops on the cathode surface, which is polarized at −0.8 VDC to insure the concentration approaches zero. For the iodine system, the range of polarization voltage is quite broad, insuring large increases in flowrate will not deplete the electron source at the cathode. Details concerning the downstream electronics and calibration associated with this measurement technique are to be found elsewhere (Zabaras *et al.* 1986).

It is now recognized (Mao & Hanratty 1985) that the response of the electrochemical probe is highly dependent of the nature of the "input" wall shear stress. For the ionic system employed in this study, errors in both phase and magnitude are expected to be small due to the large (10^3 s^{-1}) mean velocity gradient, small cathode surface area and large Schmidt number (ν/D) of the fluid (≈ 780). The relationship given by Hanratty & Campbell (1983) between cathode current and wall shear stress was used in this study, as the frequencies in the data were sufficiently low to allow the use of a quasi-steady analysis.

Data collection, processing and analysis

Voltage signals from two film thickness probes and the wall shear stress probe were first low-pass filtered at 1 kHz, then fed to a microcomputer-based A/D converter. Each signal was digitized at 1 kHz by a data translation 12-bit A/D converter installed in a DEC Micro 11/73 microcomputer. The data set comprised 1 min of data, and was stored on the system Winchester disc prior to applying calibration curves and writing the data to magnetic tape for further analysis. Digitization and collection errors are expected to be negligible for all data, while calibration errors for the film thickness measurement are expected to be $<3\%$. Errors inherent in applying steady-state wall shear stress calibration curves depend on the nature of the input signal, requiring separate examination of individual results. Zabaras (1985) reports estimated errors of $<7\%$ for this technique.

Film thickness and wall shear stress data was examined to locate typical interacting or evolving waveforms. Due to the limited amount of data provided by the two film thickness probes, determining the evolutionary character of waveforms was difficult. However, several types of wave shapes appeared frequently, although their individual dimensions varied considerably. Four waveforms were chosen as representative of the large wave structures, each having peak thicknesses greater than twice the surrounding substrate thickness. In addition, each was preceded by a reasonably smooth substrate, shown by wall shear stress measurements to be free of acceleration.

Each measured film thickness profile was converted from the time domain into a spatial domain for use with the numerical algorithm. Wave peak passage times between probes were used to estimate "wave velocities"—these values provided initial estimates for the numerical computations.

NUMERICAL METHOD

Solution of free boundary problems requires methods for both hydrodynamic calculations and shape determination. The velocity and pressure fields within the wave were determined by solving the Navier–Stokes equations in primitive variable form. For a film Reynolds number of 880, the wave thickness generally was $<1\%$ of the pipe radius and therefore, a two-dimensional cartesian coordinate system was chosen. The transformation of time traces of film thickness to this coordinate system comprised the shape determination portion of the overall algorithm. The common method of computing the free surface position is to compute film thickness values at fixed streamwise locations. The present work inverts this procedure; for a measured sequence of film thickness values, streamwise locations associated with each value are determined such that the resulting shape and flow field within satisfies all interfacial boundary conditions.

To develop the methodology for treating evolving films, waves were initially modeled as though their shape remained constant with time—these waves are termed solitary. A new streamwise coordinate, z, is fixed on the front of the wave and extends in the opposite direction of gravity. The film thickness profile in the time domain, $h(t_i)$, was converted to the length domain, $h(z_i)$, through the transformation

$$z_i = z_0 + V_w(t_i - t_0), \qquad [1]$$

for i ranging from 1 to the number of film thickness points in the isolated wave. Through this transformation, the wave profile was "stretched" for use as a computational domain, and time was removed from the problem. In this coordinate system, the wave remains fixed, and the wall moves upward at a constant speed given by V_w, the wave velocity for the solitary wave.

It is useful to define a new streamwise velocity component,

$$u(z, y) = -u'(x, y, t) + V_w, \qquad [2]$$

where $u'(x, y, t)$ is the streamwise velocity in a coordinate system fixed on the wall. The governing equations for this viscous, incompressible and isothermal flow relative to the moving wave become

$$u\frac{\partial u}{\partial z} + v\frac{\partial u}{\partial y} = -\frac{1}{\rho}\frac{\partial P}{\partial z} - g + \nu\left(\frac{\partial^2 u}{\partial z^2} + \frac{\partial^2 u}{\partial y^2}\right), \qquad [3]$$

$$u\frac{\partial v}{\partial z} + v\frac{\partial v}{\partial y} = -\frac{1}{\rho}\frac{\partial P}{\partial y} + \nu\left(\frac{\partial^2 v}{\partial z^2} + \frac{\partial^2 v}{\partial y^2}\right) \qquad [4]$$

and

$$\frac{\partial u}{\partial z} + \frac{\partial v}{\partial y} = 0, \qquad [5]$$

where v is the velocity in the normal (y) direction, P is the pressure, g represents gravitational acceleration and ν and ρ are the kinematic viscosity and density of the fluid, respectively. At the stress-free interface, $y = h(z)$, tangential and normal stress balances require

$$\left(\frac{\partial u}{\partial y} + \frac{\partial v}{\partial z}\right)\left[1 - \left(\frac{\mathrm{d}h}{\mathrm{d}z}\right)^2\right] - 2\frac{\mathrm{d}h}{\mathrm{d}z}\left(\frac{\partial u}{\partial z} - \frac{\partial v}{\partial y}\right) = 0 \qquad [6]$$

and

$$P = \sigma\frac{\dfrac{\mathrm{d}^2 h}{\mathrm{d}z^2}}{\left[1 + \left(\dfrac{\mathrm{d}h}{\mathrm{d}z}\right)^2\right]^{3/2}} + \frac{2\mu}{1 + \left(\dfrac{\mathrm{d}h}{\mathrm{d}z}\right)^2}\left[\frac{\partial u}{\partial z}\frac{\mathrm{d}h^2}{\mathrm{d}z} - \left(\frac{\partial u}{\partial y} + \frac{\partial v}{\partial y}\right)\frac{\mathrm{d}h}{\mathrm{d}z} + \frac{\partial v}{\partial y}\right], \qquad [7]$$

where σ is the surface tension coefficient and μ is the absolute viscosity. At the wall, $y = 0$,

$$u = V_w, \qquad v = 0, \tag{8}$$

represent the standard no-slip and no-flux conditions.

Velocities at the interface are related through the kinematic condition in a moving frame,

$$v = u\frac{dh}{dz}. \tag{9}$$

The inlet velocity profile is parabolic, representing an acceleration-free falling film, while a sufficient and physically consistent outlet condition for a solitary wave requires a zero streamwise derivative for all variables. The variable V_w replaces $h(z)$ as the final variable to be iteratively determined in the free surface problem.

For each wave profile, a unique, non-uniform finite difference grid mesh was constructed. The mesh for a typical domain is shown in figure 3. The particular wave shape determined the grid spacing used. Mesh refinement continued until no further change in either the computed wave velocity or wall shear stress profile was observed. Of particular importance was the concentration of cells near the front of the wave, since the velocity fields change drastically in this region due to the large interfacial slope. In addition, large curvatures exist at each peak and trough. To insure adequate resolution of capillary pressure induced effects, grids were concentrated near the free interface in these regions. For most waves, 1800 cells of dimension $\delta x\,\delta y$ were sufficient, and produced grid Reynolds numbers [$\mathrm{Re}_{Gx} = u(z, y)\,\delta x/v$, $\mathrm{Re}_{Gy} = v(z, y)\,\delta y/v$] of order 1 in the y direction, and ranging from 1 to 100 in the streamwise direction.

The curved interface was accomodated by allowing boundary cells to be cut by the boundary, $h(z)$, thus reducing their volume. This situation is illustrated in figure 4. This technique produced areas adjoining two boundary cells, the centers of which were outside the computational domain. As the stress-free interface requires a zero normal derivative of the velocity vector with respect to the boundary, $h(z)$, these regions were treated as inviscid channels through which all fluid leaving one boundary cell on its shared side passed into the neighboring cell through its respective shared side. The total area of these regions represents $<0.1\%$ of the total domain, and had little effect on the results.

The equation set was solved on a finite difference grid using a variant of the TEACH-T code (Gosman *et al.* 1969), incorporating the SIMPLER pressure/continuity solution procedure; the principles of this method are described in detail elsewhere (Patankar 1980). The domain includes regions of significant streamwise variation in all variables, thus necessitating an accurate method of discretizing convective momentum terms. The simplest method of convective discretization, upwind differencing, ensures a reasonably stable numerical solution, but introduces numerical diffusion in regions of the flow where streamlines are oblique with respect to the grid lines (Raithby 1976). More importantly, the upwind scheme lacks sensitivity to cross-stream diffusion and source terms (Leonard 1979), which are of tremendous importance in the case of a thin film.

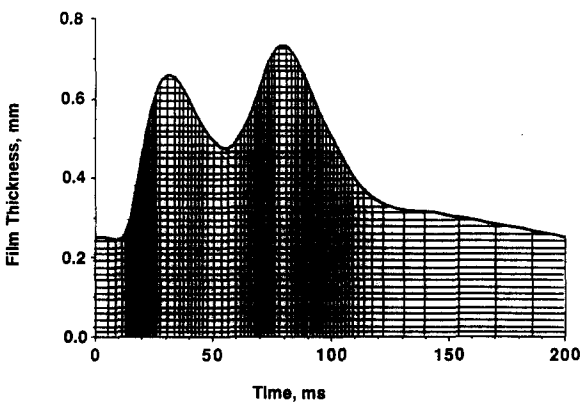

Figure 3. Sample finite difference grid.

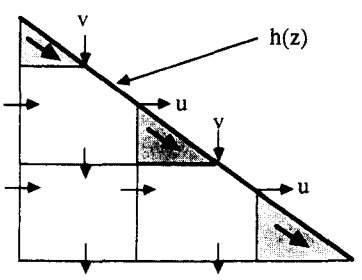

Figure 4. Interface finite difference grid.

This lack of sensitivity diminishes the effects of the y direction diffusion as well as the "v" velocity in the solution of the streamwise velocity. These deficiencies in the upwind and hybrid methods require the use of a QUICK-based scheme, which improves acccuracy by expanding the number of neighboring points included in interpolated values of velocity. Based on Leonard's (1979) third-order accurate discretization scheme QUICK, Pollard & Siu (1982) developed the QUICK-ER (Extended and Revised) method of discretizing convective terms. The QUICK-ER method overcomes stability problems inherent in the QUICK procedure at the expense of slower convergence, and is considered the most satisfactory method of handling convective momentum terms (Huang *et al.* 1985). For application to non-uniform grids, a new version of QUICK-ER was developed. This method follows the spirit of the QUICK-ER formulation, but includes locally variable weighting factors to account for the non-uniformity of the grid in both directions. Although QUICK-ER schemes requires more computational effort per iteration than upwinding, particularly for non-uniform grids, improvements in accuracy allow the use of a slightly coarser grid, so total computational time exceeds that required by the upwind method by only 20%.

The solution procedure began with choosing a value for V_w and creating the transformed domain, given by [1]. The u velocity field was set to a parabolic profile everywhere, and the v velocity field was set to zero. The pressure at each z location was set to the surface pressure due to curvature. Updated velocity and pressure fields within the wave were then computed using [3]–[5]. Through interpolation for the velocity gradients in the interfacial shear stress balance, [6], streamwise and normal velocities in the interior of the flow field were used to derive an expression for the streamwise surface velocity. Coupled with the kinematic condition [9], the velocities on the surface were known for each iteration. The surface pressure computed from [7] was used to determine the first pressure value in the interior of the domain through the use of parabolic interpolation using the surface pressure and two interior pressures. With the newly computed surface variables, the velocity and pressure fields were updated until the sum of residuals of mass and momentum (normalized by the inlet quantities) over the domain was $<10^{-3}$. In addition, the interfacial shear and normal stress balances were required to be within 10^{-2} Pa of zero.

The free boundary shape was determined by examining the converged average outlet pressure in the flat film section. If the average pressure did not approach zero, as required for a non-accelerating film trailing a solitary wave, a new value of V_w was chosen and the process repeated. The adjustment procedure for V_w was simple—if the pressure in the outlet section was higher than zero, the wave (wall) velocity was too high, since the wall was pushing excess fluid through the wave, and a positive pressure at the outlet was opposing this extra fluid in an attempt to satisfy the mass balance for the wave.

The numerical study of evolving or interacting waves retains much of the methodology developed for solitary waves, differing only in the wave shape determination. Examination of the experimental measurements of film thickness reveals the large waves change rapidly between the upper and lower film thickness probe. The waves appear to change from solitary type waves by being perturbed by locally variable mass and momentum sources, physically recognized as small waves. Incorporating this unsteady effect is accomplished through the use of a locally constant stretching parameter, as opposed to the globally constant value used for the classical solitary wave. The domain transformation for this case is given by

$$z_i = z_0 + V_{w,i}(t_i - t_0), \qquad [10]$$

where z is the streamwise coordinate fixed on the wave front. In general, this pseudo wave velocity is

$$V_{w,i} = V_w[1 + e(z_i)], \qquad [11]$$

where $e(z_i)$ is an iteratively determined local stretching variable and V_w represents the wave velocity associated with the substrate. The solitary wave case is recovered by setting $e(z_i) = 0\ \forall i$. As before, we define a new streamwise velocity component as

$$u(z, y) = -u'(x, y, t) + V_w(z_i). \qquad [12]$$

This transformation introduces locally variable mass and momentum sources into the u momentum and continuity equations [3] and [5], which become

$$u\left(\frac{\partial u}{\partial z}+\frac{\mathrm{d}V_w}{\mathrm{d}z}\right)+v\frac{\partial u}{\partial y}=-\frac{1}{\rho}\frac{\partial P}{\partial z}-g+\nu\left(\frac{\partial^2 u}{\partial z^2}+\frac{\partial^2 u}{\partial y^2}-\frac{\mathrm{d}^2 V_w}{\mathrm{d}z^2}\right) \quad [13]$$

and

$$\frac{\partial u}{\partial z}+\frac{\partial v}{\partial y}-\frac{\mathrm{d}V_w}{\mathrm{d}z}=0. \quad [14]$$

The interfacial stress conditions [6] and [7] are modified slightly by the unsteady effects, and become

$$\left(\frac{\partial u}{\partial y}+\frac{\partial v}{\partial z}\right)\left[1-\left(\frac{\mathrm{d}h}{\mathrm{d}z}\right)^2\right]-2\frac{\mathrm{d}h}{\mathrm{d}z}\left(\frac{\partial u}{\partial z}-\frac{\partial v}{\partial y}-\frac{\mathrm{d}V_w}{\mathrm{d}z}\right)=0 \quad [15]$$

and

$$P=\sigma\frac{\dfrac{\mathrm{d}^2 h}{\mathrm{d}z^2}}{\left[1+\left(\dfrac{\mathrm{d}h}{\mathrm{d}z}\right)^2\right]^{3/2}}+\frac{2\mu}{1+\left(\dfrac{\mathrm{d}h}{\mathrm{d}z}\right)^2}\left[\left(\frac{\partial u}{\partial z}-\frac{\mathrm{d}V_w}{\mathrm{d}z}\right)\frac{\mathrm{d}h^2}{\mathrm{d}z}-\left(\frac{\partial u}{\partial y}+\frac{\partial v}{\partial y}\right)\frac{\mathrm{d}h}{\mathrm{d}z}+\frac{\partial v}{\partial y}\right)\right]. \quad [16]$$

The normal stress balance, [16], was found to be insensitive to the additional term, $\mathrm{d}V_w/\mathrm{d}z$, and the term was removed from the formulation. The solution procedure for the pseudo-unsteady equations [13], [4] and [14], subject to [15] and [7]–[9], is identical to that of the solitary wave, with the exception that now a profile of $V_{w,i}$ must be specified instead of a single value. When the velocity and pressure fields have converged for a given set of $V_{w,i}$, the wave shape is adjusted through $e(z_i)$ to meet two criteria. The baseline wave velocity, V_w, is adjusted such that the average pressure in the flat outlet section approaches zero, as before. The computed wall shear stress profile is then compared to the experimental profile, and adjustments made to $e(z_i)$ to correct deviations. Upon arriving at the correct distribution of $e(z_i)$, the solution includes the velocity and pressure fields within the wave, as well as the relative extents of its evolution throughout the wave. Each solution is unique, and the wall shear stress matching procedure insures the accuracy of the velocity fields.

The procedure developed for the solitary waves required an average of 300 iterations of the velocity and pressure fields to converge, with an under-relaxation factor of one-half used for all variables. Between 4 and 8 adjustments to the solitary wave velocity were required to produce a flow with an average outlet pressure $< 10^{-2}$ Pa. For the quasi-unsteady case, roughly 500 iterations were required to achieve convergence of the velocity and pressure fields, due to the extra stiffness imposed by the multiple peaks and valleys. Adjustment of the variable wave velocity to match the wall shear stress data took anywhere from 20 to 40 iterations.

The program was coded in FORTRAN 77, and required 2 mbyte of task space. Execution times for convergence of the velocity and pressure fields for a given wave shape were approx. 5 CPU h on a VAX 11-750.

RESULTS

This study concentrated on waves developing from or interacting with isolated waves, identified by comparing film thickness measurements from both upper and lower probes. Examination of the experimental film thickness data shows that many large waves fall into three categories. While nearly solitary waves exist, few are free from small wave induced ripples, an example of which is shown in figure 5. As the wave travels from the upper to the lower probe, the small hump on the wave tail grows, while the wave front retains its structure; we classify this wave as type A. Large waves appear susceptible to splitting when perturbed, as illustrated in figure 6. These waves, classified as type B, cover a large portion of the interface, and suggest that modeling falling films far from the inlet as steady processes neglects important dynamics. The interaction of two large waves of unequal size is shown in the wave trace in figure 7. Although significantly smaller, the trailing wave seen in the upper trace either passes through the larger wave or accumulates a larger

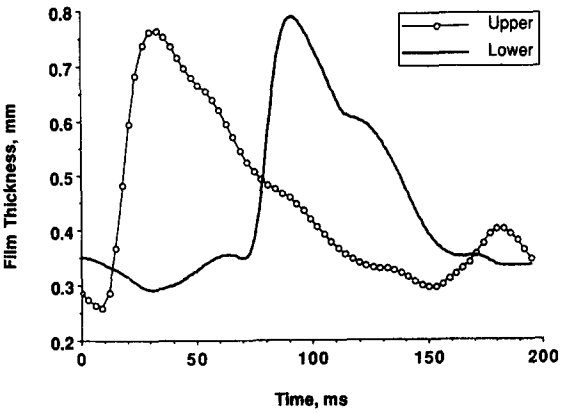

Figure 5. Evolution of a nearly solitary wave: type A.

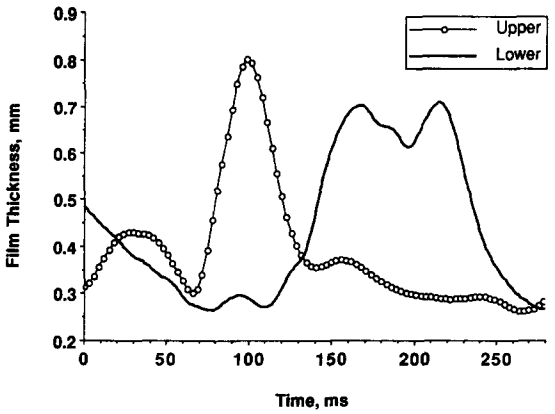

Figure 6. Evolution of a large wave via splitting: type B.

portion of its mass, leading to a situation classified as type C. While each of these cases characterizes a significant fraction of the interface, combinations of these effects are also seen. Figure 8 illustrates the splitting of a large wave coupled with the interaction of the large wave with a small wave preceding it. This type D wave is not representative of all complicated waves, but serves as an example of the combination of evolution and interaction effects.

Description of large waves is generally limited to peak and substrate thicknesses and wavelengths. Experimental data is limited to two time traces of film thickness, which makes quantitative evaluation of these variables difficult. It must suffice to characterize the extent of evolution by the time separation of individual peaks, while the relative mass of each peak is estimated on the basis of the peak thickness. In conjunction with the numerical predictions of flow fields, these data offer new insight into the hydrodynamic processes occurring in the large waves.

Streamlines computed for the type A wave are shown in figure 9. The presence of a large recirculation region is seen within the peak of the wave when viewed in a coordinate system fixed on the wave. The interaction of this large mass of fluid with the surrounding substrate results in regions of strong streamwise acceleration ahead and behind the region. These results were also seen in studies of nearly solitary waves with similar peak/substrate thickness ratios (Wasden & Dukler 1989). The presence of the growing hump on the wave tail increases the size of the recirculation region, compared to a solitary wave, which causes larger disruptions in the substrate as the wave peak passes over. The wall shear stress profile for this wave is shown in figure 10, along with experimental values. Agreement is excellent over most of the wave—the experimental values at the tail suggest outside or cross-stream disturbances are present. This discrepancy is not expected to significantly alter the overall flow field, as the region under the peak is insensitive to downstream disturbances at $\mathrm{Re} = 880$. Matching the wall shear stress data required stretching the wave shape in transforming it from the time domain to the spatial domain, as shown in figure 11. The transformation required that the entire wave stretch in length, compared to a purely solitary wave; the magnitude of $e(z_i)$, [11], is shown in figure 11. Of special interest is the extra stretching caused by the presence of the hump on the tail—previous studies of nearly solitary waves (Wasden & Dukler 1989) show the evolution is confined to the region very near the peak, while in this case, the tail region is stretching as well. From a substrate wave velocity of 1.10 m/s, the wave velocity $V_{w,i}$, [11], increased to 1.89 m/s near the peak. The average, or Nusselt, film velocity for this Re (Kapitza 1964) is 0.51 m/s, showing the wave moves at between 2.1 and 3.7 times the average velocity. The combination of experimental observations and numerical simulations show that the wave is in the early stages of splitting, and that this effect, although seemingly slight upon examining the film thickness measurements, significantly affects the flow field.

Flow within a wave with the peak splitting into daughter waves is shown in figure 12. The flow beneath each peak resembles that seen in the nearly solitary wave A. The recirculating region encloses the entire area under the twin peaks, and again causes large accelerations near the front and rear of the wave. The remnants of the original solitary wave recirculation region are seen at

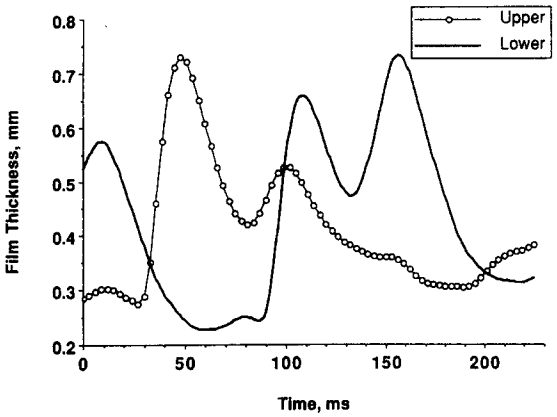

Figure 7. Interaction of large waves: type C.

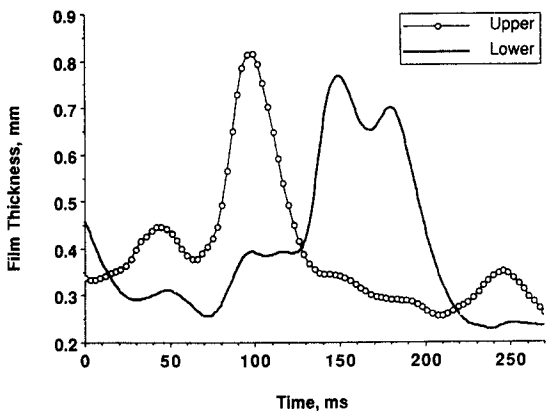

Figure 8. Evolution and interaction of large waves: type D.

the front of the wave, with the newly formed rear peak having a smaller recirculation region, even though it has a roughly equivalent peak thickness. This observation demonstrates the danger of classifying multiple waves based solely on the easily measured parameters such as peak thicknesses and separation time. Comparison of computed and measured wall shear stress is shown in figure 13 to be excellent. The peak in wall shear stress preceding the first peak in film thickness is similar to that observed in an isolated wave, showing how the evolving wave retains part of its original traits. The second shear stress peak is a further indication of the emergence of a new peak. The domain and stretching parameter variation for this wave are shown in figure 14. The stretching parameter was varied such that the peaks were evolving most rapidly, with the trough moving slower than either peak. As expected, the second peak was moving slightly ($\approx 10\%$) slower than the first. The substrate wave velocity was 1.32 m/s, yielding $V_{w,i}$ from 1.32 to 1.91 m/s under the peaks. Compared to the Nusselt velocity, the wave moves roughly 2.6–3.8 times faster.

Flow in an interacting wave sequence is shown in figure 15. The two waves appear to have independent recirculation regions, with the first preceded by the characteristic acceleration region. The size of the recirculation zones appears to be related to the thicknesses of the individual peaks, in contrast to the evolving case, type B. This may result from the extra separation that exists in this case, causing speculation that the type B wave would evolve into a wave similar to type C. Shear stress profiles for the interacting case are displayed in figure 16. The agreement between computed and measured shear stress is excellent, and shows two peaks in shear stress, indicating the wave is evolving into two nearly solitary waves. As the wave peaks separate further, the second wall shear stress peak is closer in magnitude to that expected of an isolated wave, additional evidence of future disintegration of the original wave. The transformed domain and stretching parameter variation are shown in figure 17. Both peaks were evolving at a nearly identical rate, suggesting the effect of the interactions on the natural evolution of the wave was slight. As was

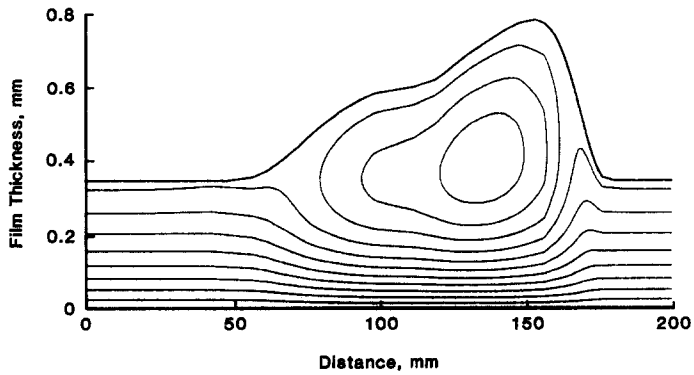

Figure 9. Streamline map: wave A.

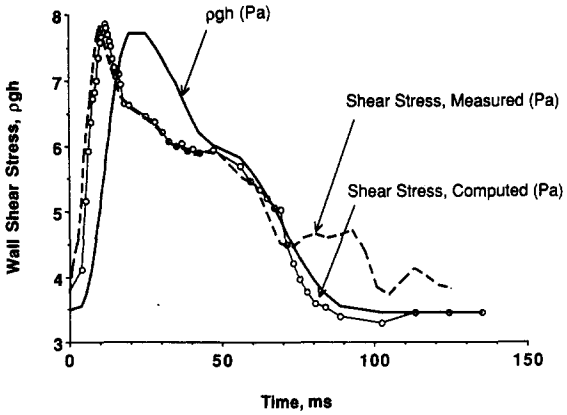

Figure 10. Shear stress comparison: wave A.

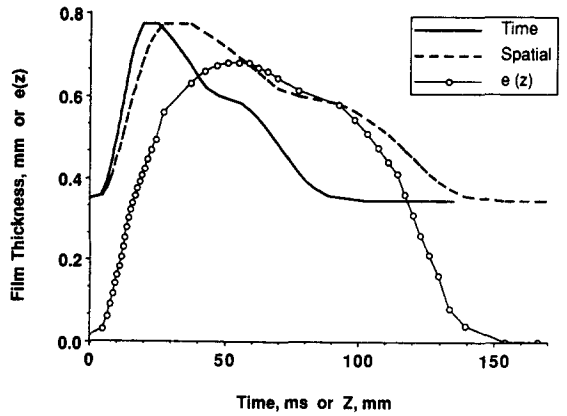

Figure 11. Experimental and computed wave shape: wave A.

previously the case, the trough between the waves was stretching more slowly than the peak regions. The substrate wave velocity was 1.12 m/s, closer to the solitary wave (A) than the splitting wave (B). The wave velocity, $V_{w,i}$, varied from 1.12 to 1.7 m/s under the peaks, roughly 2.1–3.3 times the Nusselt velocity.

The most complicated waveform studied included the effects of evolution and interaction. Flow within this wave, classified as type D, is shown in figure 18. Apparently the interaction of the large wave structure with the small wave near the front has little effect on the overall flow pattern, compared to what occurs in simple evolving waves of this size (see figure 12). A region of moderate acceleration exists at the front of the small forerunner wave, followed by a region of nearly parallel flow. This flow profile suggests the effect of the initial interaction is limited to accelerating fluid away from the wall, and effectively changing the substrate thickness with which the large wave interacts. Further downstream, the large acceleration region is again evident, due to the interaction of the large recirculation region with the slowly moving substrate. As the wave has only begun to evolve, the recirculation region is reminiscent of that associated with a stretched isolated wave, although the area near the trough of the wave implies future separation of the waves. Shear stress data for this wave is shown in figure 19; agreement between the measured and computed values is excellent over the entire wave. The shear stress profile provides further evidence of the dampening effect of the interaction of the large wave with the small forerunner wave. The maximum shear stress preceding the large wave peak is smaller (relative to ρgh) than existed in the previous cases. This may be due to the relative difference in size between the wave peak and the local substrate—previously, wave peak/substrate ratios were ≈ 3, while the ratio between the first peak and the plateau preceding it, in this case, is <2. Since the splitting of the peaks has just begun, no significant secondary peak in shear stress exists. The transformed domain and stretching

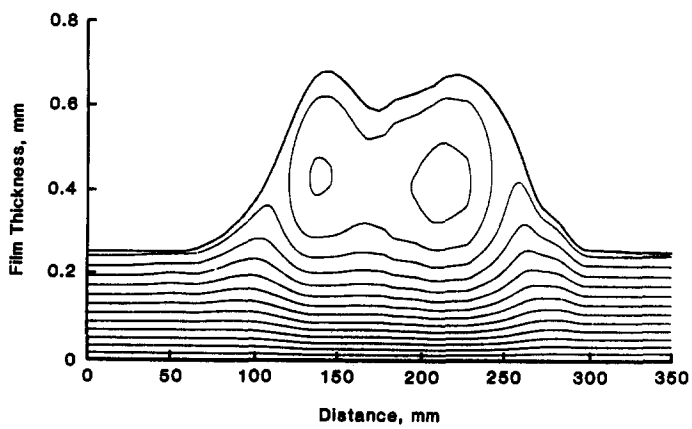

Figure 12. Streamline map: wave B.

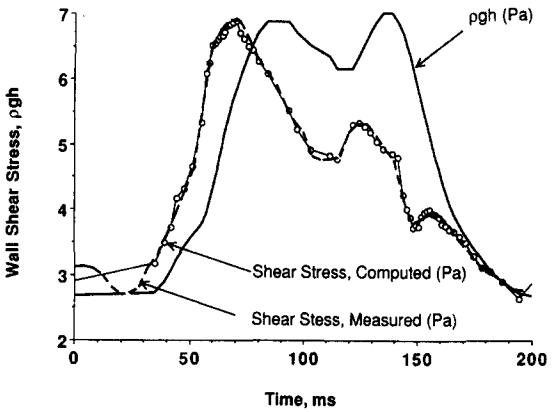

Figure 13. Shear stress comparison: wave B.

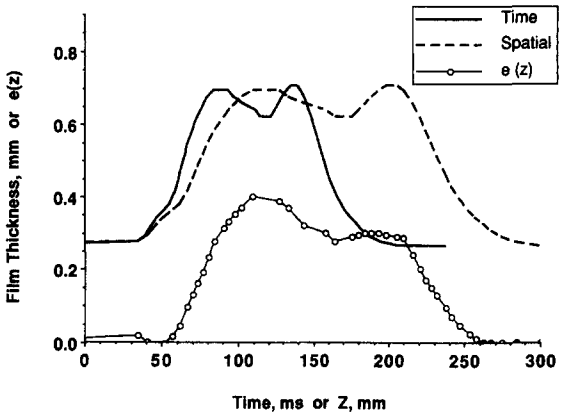

Figure 14. Experimental and computed wave shape: wave B.

parameter variation are shown in figure 20, and are similar to cases B and C. Evolution of the forerunner wave is significant; the wave is stretching out in response to the mass descending on it. As before, the second peak is moving slightly slower than the first ($\approx 5\%$); from data shown in case B, the difference is expected to increase with the extent of evolution. From a substrate wave velocity of 1.24 m/s, the wave velocity $V_{w,i}$ increased to 1.89 m/s under the peak, ranging from 2.4 to 3.8 times the Nusselt velocity.

SUMMARY AND CONCLUSIONS

Interacting or evolving large waves comprise a large portion of the interface of a falling liquid film. Wave amplitudes of 2–5 times the substrate thickness are common even for moderate Reynolds numbers, ruling out models based on small perturbation theory. From film thickness measurement time traces, four representative large waves were selected as comutational domains for a numerical solution of the Navier–Stokes equations. Computed results included velocity and pressure fields, as well as the wave shape necessary to match shear stress measurements. Values of $V_{w,i}$ [11], remain near those expected for solitary waves with similar peak and substrate thicknesses, as reported by Wasden & Dukler (1989). The stretching technique developed for this study allowed simple accomodation of local unsteady effects by decoupling the hydrodynamic and shape determination problems. An interesting extension of the present work would be to measure the film thickness at several closely spaced locations, and attempt to compute $e(z)$ from the data.

The bulk of the liquid in large interacting or evolving waves is carried in the region above the substrate, and is nearly stationary in a coordinate system moving with the wave. As the wave moves rapidly over the slow substrate, it causes acceleration of fluid from the front into the peak. The

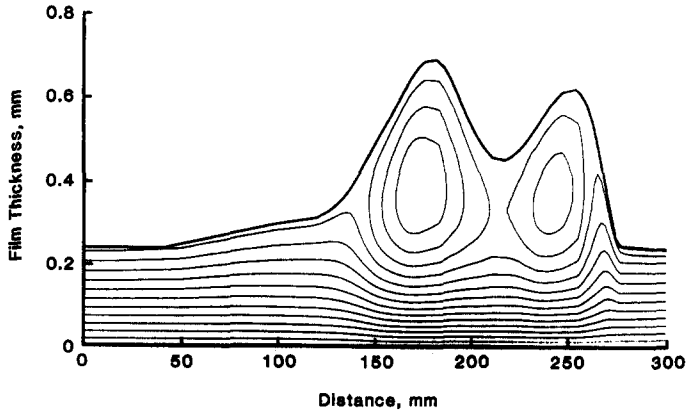

Figure 15. Streamline map: wave C.

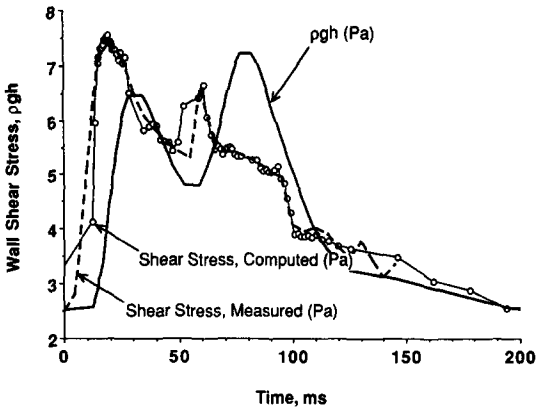

Figure 16. Shear stress comparison: wave C.

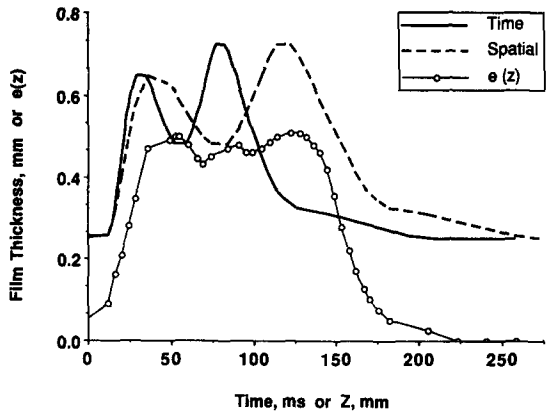

Figure 17. Experimental and computed wave shape: wave C

fluid then decelerates as it passes out of the wave tail, generating a closed recirculation region in the wave peak. Waves with multiple peaks have multiple regions of recirculation, with mixing zones between them. These regions occur only in multiple-peak waves, and may be responsible for heat and mass transfer enhancement above that due to fluid acceleration and circulation. The magnitude of the enhancement due solely to multiple wave interactions is unknown, but may be significant compared to that associated with isolated large waves. The computations were limited to waves having two peaks, but these results are expected to extrapolate well for cases of more than two

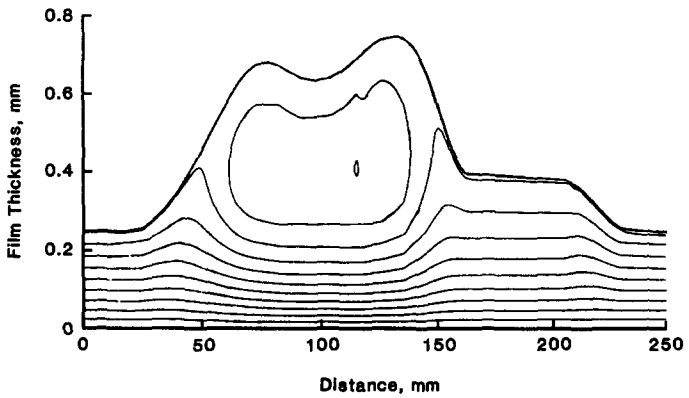

Figure 18. Streamline map: wave D.

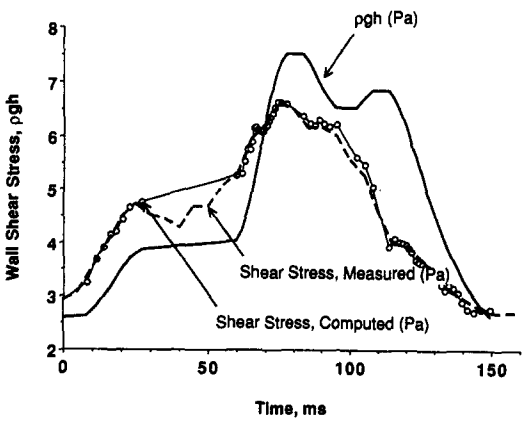

Figure 19. Shear stress comparison: wave D.

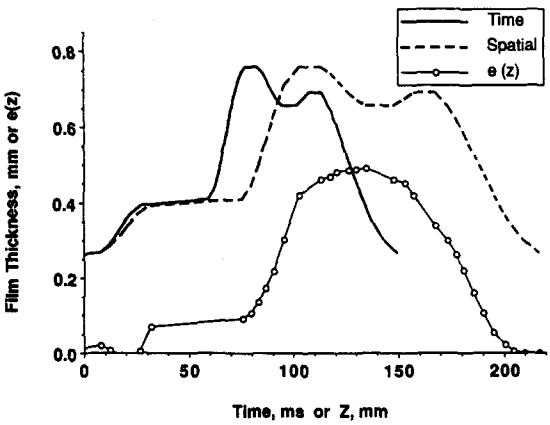

Figure 20. Experimental and computed wave shape: wave D.

peaks. As a majority of the surface is covered by evolving or interacting waves, further efforts toward determining relative effects of competing hydrodynamic processes is justified.

Perhaps the most surprising result of this study concerned the similarity between flow fields resulting from the interaction of large waves and those generated by the splitting of a large wave into two waves. This similarity suggests the shape of the interface controls the fluid dynamics within, regardless of the evolutionary process from which the wave resulted. This may simplify further analyses of transport processes, and allow characterization based primarily on peak and substrate thicknesses, as well as separation times.

Modeling large wave interactions will require the use of velocity profiles capable of representing the large streamwise accelerations existing in the flow. Previous work (Wasden & Dukler 1989) has shown a cubic polynomial reasonably approximates the normal (y) variation of the streamwise velocity at all axial locations: its use for modeling the evolution of large waves is recommended.

Acknowledgements—Financial support for this research by the Office of Naval Research is gratefully acknowledged. One of the authors (F.K.W.) was supported by a National Science Foundation Graduate Fellowship.

REFERENCES

BACH, P. & VILLADSEN, J. 1984 Simulation of the vertical flow of a thin wavy film using a finite-element method. *Int. J. Heat Mass Transfer* **27,** 815–827.

BROWN, R. C., ANDREUSSI, P. & ZANELLI, S. 1978 The use of wire probes for the measurement of liquid film thickness in annular gas–liquid flows. *Can. J. chem. Engng* **56,** 754–757.

DUKLER, A. E. 1972 Characterization, effects and modelling of the wavy gas–liquid interface. *Prog. Heat Mass Transfer* **6,** 207–223.

DUKLER, A. E. 1977 The role of waves in two phase flow: some new understanding. *Chem. Engng Educ.* **1976,** 108–138 (Award Lecture).

GOSMAN, A. D., PUN, W. M., PUNCHAL, A. K., SPALDING, D. B. & WOLFSTEIN, M. 1969 *Heat and Mass Transfer in Recirculating Fluid Flow.* Academic Press, London.

HANRATTY, T. J. & CAMPBELL, J. A. 1983 Measurement of wall shear stress. In *Fluid Mechanics Measurements* (Edited by GOLDSTEIN, R. J.), pp. 559–617. Hemisphere, Washington, D.C.

HUANG, P. G., LAUNDER, B. E. & LESCHZINER, M. A. 1985 Discretization of nonlinear convection processes: a broad-range comparison of four schemes. *Comp. Meth. appl. mech. Engng* **48,** 1–24.

KAPITZA, P. L. 1964 Wave flow of thin layers of a viscous fluid. In *Collected Papers of P. L. Kaptiza,* Vol II. Macmillan, New York.

KHESHGI, H. S. & SCRIVEN, L. E. 1987 Disturbed film flow on a vertical plate. *Phys. Fluids* **30,** 990–997.

LEONARD, B. P. 1979 A stable and accurate convective modelling procedure based on quadratic upstream interpolation. *Comp. Meth. appl. mech. Engng* **12,** 59–98.

MAO, Z.-X. & HANRATTY, T. J. 1985 The use of scalar transport probes to measure wall shear stress in a flow with imposed oscillations. *Expts Fluids* **3,** 129–135.

PATANKAR, S. V. 1980 *Numerical Heat Transfer and Fluid Flow.* Hemisphere, Washington, D.C.

POLLARD, A. & SIU, A. L. W. 1982 The calculation of some laminar flows using various discretisation schemes. *Comp. Meth. appl. mech. Engng* **35,** 293–313.

RAITHBY, G. D. 1976 A critical evaluation of upstream differencing applied to problems involving fluid flow. *Comp. Meth. appl. mech. Engng* **9,** 75–104.

WASDEN, F. K. & DUKLER, A. E. 1989 Insights into the hydrodynamics of free falling films. *AIChE Jl* **35,** 187–196.

ZABARAS, G. J. 1985 Studies of vertical, annular gas–liquid flow. Ph.D. Dissertation, Univ. of Houston, Tex.

ZABARAS, G. J., MARON, D. M. & DUKLER, A. E. 1986 Vertical upward concurrent gas–liquid annular flow. *AIChE Jl* **32,** 829–843.